International Journal of Modern Physics C
Vol. 19, No. 6 (2008) 875–902

World Scientific
www.worldscientific.com

MULTI-RELAXATION TIME LATTICE BOLTZMANN MODEL FOR MULTIPHASE FLOWS

A. KUZMIN* and A. A. MOHAMAD†

Mechanical and Manufacturing Engineering
Schulich School of Engineering, University of Calgary
2500 University Drive NW
Calgary, Alberta T2N 1N4, Canada
**shurik.kuzmin@gmail.com*
†*mohamad@ucalgary.ca*

S. SUCCI

Institute for Applied Computing, IAC-CNR
Viale del Policlinico 137, 00161, Roma, Italy
succi@iac.rm.cnr.it

Received 8 January 2008
Accepted 16 January 2008

Multi-relaxation time (MRT) for Lattice Boltzmann method is gaining renewed attention among researchers in the field. The advantage of such formulation over the widely popular single-time relaxation version, is twofold: better numerical stability and wider span of physical applications, extending to non-isotropic flows. In this work, the numerical advantages of the MRT model versus single-relaxation time (BGK) operator are quantitatively assessed through direct numerical simulations of droplet formation and capillary wave propagation on interphase boundaries. The results show that by proper tuning of the collision operator, and particularly of the higher-order kinetic modes (ghosts), appreciable improvements in stability limits, of the order of 20%, and viscosity limits, of the order of 80%, can be achieved. Moreover, a theoretical analysis accounting for the reasons behind such stability improvement, is also presented.

Keywords: Multiphase; Shan–Chen model; multi-relaxation time; droplet formation; stability.

PACS Nos.: 47.11.-j, 47.35.Pq, 47.45.Ab, 47.55.-D.

1. Introduction

Lattice Boltzmann method (LBM) has emerged as a powerful competitor for conventional computational fluid dynamics (CFD) methods,[1,2] especially for the simulations of multi-phase flows and flows with complex boundary conditions.[3]

Modeling of two-phase flow with LBM goes back to the work of Gunstensen *et al.*[4] Gunstensen used color fluids to represent each phase. By introducing the

color current and gradient, the authors developed a self-consistent source term, including surface tension. However, there are few limitations of such a model, mainly the anisotropy of the surface tension and extensive demand of computer resources, even with BGK[5] single-relaxation time collision operator.[2]

Later on, He *et al.*[6] (HSD model) used series of expansion of intermolecular potential to obtain a proper force term, which accounts for multiphase behavior. He *et al.*[7] extended the HSD model to incompressible multiphase flows[7] by using two sets of distribution functions, one for the fluid pressure and velocity field, and the other to capture the interface. Hence, the phase interface is enforced to be smooth. However, serious limitations for the model application are related to the numerical instability, associated with the "stiffness" of the collision operator and to hard-core repulsive interactions.

Swift *et al.*[8] developed a model for non-ideal fluids to account for the interfacial thermodynamics, utilizing free-energy approach. The fluid is instructed to reach the right thermodynamic equilibrium under the effect of the correct non-ideal equation of state. The major drawback of this approach is that the model suffers from unphysical Galilean invariance, coming from the non-Navier–Stokes terms.[9] In addition, it does not support significant density contrasts between the light and dense phases.

Shan and Chen[10] (SC) proposed a multiphase model, where forces are directly encoded as the result of pairwise molecular interactions (pseudo-potential). In the model, an additional momentum forcing term is explicitly added to the velocity field at each time step. The model is conceptually straightforward and easy to use, which explains its increasing popularity. However, the model is not consistent with thermodynamic behavior and can only handle moderate liquid-vapor density ratios.[11]

Luo[12] and Lee and Lin[13] also introduced finite density and pressure-based multiphase models, respectively. However, none of these models seems to have received significant attention.

A comprehensive review on the applications of LBM for complex and multiphase flows is available.[9]

Almost all multiphase models experience instabilities and spurious currents, due to the lack of high-order isotropy of the lattice (beyond the fourth order needed to recover the correct momentum-flux tensor for ideal gases). For simplicity, most applications use BGK, single-relaxation time model.[5] However, single-relaxation time model suffers from numerous drawbacks, instability, unsteadiness, inability to simulate problems with Prandtl number different than order of unity. Further steps have been taken by introducing multi-relaxation time (MRT) and two relaxation time (TRT) models for collision operator.[14–16] These models showed better stability, steadiness, and flexibility to simulate problems with different bulk viscosities. The MRT model represents the collision operator in the matrix form. That allows to control all moments of Navier–Stokes equation (density, current fluxes), bulk viscosity, local viscosity, and Prandtl number.[14,15,17] The model contains a few free

parameters which can be adjusted to improve stability and steadiness. We refer to work of D'Humieres,[14,17] Luo,[15] Ginzburg,[16,18] Lallemand,[15] which built on the original matrix formulations of the LBM.[19,20]

MRT and TRT models have been applied by a few researchers to simulate different phenomena, such as a simulation of lid-driven cavity,[21] binary drop collisions.[22] All these simulations showed the MRT collision operator offers enhanced stability over the BGK operator. However, among the all different applications of MRT, one finds that multiphase problems are still not fully developed. Pioneering MRT work to model the multiphase flows was performed by Abraham and coworkers.[23,24] These authors incorporated the Carnahan–Starling equation of state[9,23] into the force term. Their multiphase approach is similar to the work of He *et al.*,[6] previously mentioned. The model has been tested for different multiphase flows conditions, such as capillary waves, Laplace–Young test, Lamb test. The results confirmed the superiority of MRT collision operator for high-density-ratio problems and low-viscosity fluids. Later on, Muhkerjee and Abraham[25] developed a pressure-based MRT high-density-ratio two-phase LBM, and claimed to reach density ratios up to 1000. One should also mention the work of Ginzburg, who developed a collision operator requirement on the surface of two phases.[26]

The present work adopts Shan–Chen model (SC) with MRT collision operator. SC model is easy to implement, since the effect of surface tension can be added as a source (force) term. The results show that the MRT collision operator can definitely improve the stability of Shan–Chen model simulations. In addition, the matrix SC model has a few more degrees of freedom to simulate other physical phenomena, such as anisotropic droplet formation.

Our results show that the use of MRT Shan–Chen achieves tangible gains over the standard BGK; the compressibility can be increased by about 10% and the viscosity limit improved substantially about 20%.

This paper is organized as follows: first a brief introduction to the LBM theory, BGK collision operator, and force incorporation are given. Then, the Shan–Chen model is described, followed by the MRT collision operator. The results of numerical experiments are presented and discussed. Finally, the main findings and suggestions for further work are included in the conclusion section.

1.1. *Boltzmann equation*

It is well known that the Botlzmann equation (1) can recover the Navier–Stokes equation (2) for fluid flow. The Boltzmann equation can be written as:

$$\frac{\partial f}{\partial t} + \boldsymbol{v}\frac{\partial f}{\partial \mathbf{r}} + \mathbf{F}\frac{\partial f}{\partial \boldsymbol{v}} = \Omega\,, \tag{1}$$

where Ω is the collision operator, which represents the collision between particles; f is the particle distribution function in the space $(\mathbf{r}, \boldsymbol{v}, t)$. Navier–Stokes equation

has the following form:

$$\rho\left(\frac{\partial \boldsymbol{\upsilon}}{\partial t}+(\bar{\upsilon}\cdot\bar{\nabla})\bar{\upsilon}\right)=-\bar{\nabla}p+\rho\bar{g}+\beta\Delta\bar{\upsilon}\,. \tag{2}$$

Boltzmann equation (1) represents all possible directions of particle velocities. However, to restore macroscopi equations for fluid flow, a few selected directions are sufficient, as far as isotropy is concerned. Due to simplicity of the underlying lattice and the fact that information moves along fixed directions at a constant speed, it is easy to implement flow through complex geometry objects such as obstacles, elbows, etc.

1.2. *Discretization and BGK approximation for the LBE*

The collision operator can be represented in the so-called BGK form:[5]

$$\Omega=-\frac{f-f^{\mathrm{eq}}}{\tau}\,,$$

where $f^{\mathrm{eq}}=(1/(2\pi T)^{D/2})\exp(-(\boldsymbol{\upsilon}-\mathbf{u})^2/2T)$ is the equilibrium distribution function with mean local velocity $\mathbf{u}$ and temperature T, while τ represents the characteristic time over which the distribution function decays to the equilibrium distribution function.

Once the collision operator is chosen, it can be shown that the discretized version of Boltzmann equation (3) can recover the Navier–Stokes equation (2) by choosing the local equilibrium function in a specific manner (4). The Lattice Boltzmann equation (LBE) is presented below

$$f_i(\mathbf{r}+\mathbf{c_i}\Delta t,c_i,t)-f_i(\mathbf{r},\mathbf{c_i},t)=-\frac{f_i(\mathbf{r},\mathbf{c_i},t)-f_i^{\mathrm{eq}}(\mathbf{r},\mathbf{c_i},t)}{\tau}\Delta t\,. \tag{3}$$

Kinematic viscosity of fluid can be related to relaxation time as, $\nu=c_s^2(\tau-\Delta t/2)$, where Δt is the discretization time step. The equilibrium function is obtained from the series expansion of Boltzmann equilibrium distribution function in the Mach number $Ma=u/c_s$, where c_s is the sound velocity

$$f_i=w_i\rho\left(1+\frac{u_\alpha c_{i\alpha}}{c_s^2}+\frac{Q_{i\alpha\beta}}{2c_s^4}\right)\,, \tag{4}$$

where

$$w_i=\begin{cases}\dfrac{4}{9} & \text{if } i=0\,,\\[2mm] \dfrac{1}{9} & \text{if } i=1,\ldots,4\,,\\[2mm] \dfrac{1}{36} & \text{if } i=5,\ldots,9\,,\end{cases} \tag{5}$$

and $Q_{i\alpha\beta}=c_{i\alpha}c_{i\beta}-c_s^2\delta_{\alpha\beta}$.

The left-hand side of the LBE (3) is the so-called streaming operator, the right-hand side is a collision operator. The streaming operator governs particles which move along the lattice directions c_i. For the D2Q9 model the discrete velocities are

$$\begin{aligned} c_0 &= (0,0)\,, & c_1 &= (1,0)\,, & c_2 &= (0,1)\,, \\ c_3 &= (-1,0)\,, & c_4 &= (0,-1)\,, & c_5 &= (1,1)\,, \\ c_6 &= (-1,1)\,, & c_7 &= (-1,-1)\,, & c_8 &= (1,-1)\,. \end{aligned}$$

The collision operator defines the distribution function as it relaxes to its equilibrium state.

1.3. *Force incorporation*

The LBE (3) can simulate a host of new fluid phenomena, by incorporating appropriate force terms.

The zeroth, first, and second moments of the force term in BE (1) can be integrated and yield:

$$\int \frac{\mathbf{F}}{m}\frac{\partial f}{\partial \boldsymbol{v}}d\boldsymbol{v} = 0\,, \tag{6}$$

$$\int \frac{\mathbf{F}}{m}\boldsymbol{v}\frac{\partial f}{\partial \boldsymbol{v}}d\boldsymbol{v} = \mathbf{F}\,, \tag{7}$$

$$\int \frac{\mathbf{F}}{m}\upsilon_\alpha\upsilon_\beta\frac{\partial f}{\partial \boldsymbol{v}}d\boldsymbol{v} = \frac{F_\alpha u_\alpha + F_\beta u_\alpha}{2}\,. \tag{8}$$

Let us represent the force in a form analogical to equilibrium function:

$$S_i = w_i\left(S^0 + \frac{S^1_{i\alpha}c_{i\alpha}}{c_s^2} + \frac{S^2_{i\alpha\beta}}{2c_s^4}[c_{i\alpha}c_{i\beta} - c_s^2\delta_{\alpha\beta}]\right)\,. \tag{9}$$

Hence, by comparing (9) with (6)–(8), we obtain the following relationships:

$$\sum S_i = 0\,,$$

$$\sum S_i c_{i\alpha} = F_\alpha\,,$$

$$\sum S_i Q_{i\alpha\beta} = \frac{F_\alpha u_\beta + F_\beta u_\alpha}{2}\,.$$

To satisfy these equations, the following condition should be enforced $S^0 = 0$, $S^1_{i\alpha} = F_\alpha$, $S^2_{i\alpha\beta} = F_\alpha u_\beta + F_\beta u_\alpha/2$. Therefore, the force term can be incorporated within the equilibrium function, as follows:

$$\tau S_i + f_i^{\mathrm{eq}} = w_i\left(1 + \frac{c_i}{c_s^2}\left(\frac{\tau F_a}{\rho} + u_\alpha\right) + \frac{Q_{i\alpha\beta}}{2c_s^4}\left(\frac{F_\alpha\tau}{\rho}u_\beta + \frac{F_\beta\tau}{\rho}u_\alpha + u_\alpha u_\beta\right)\right)\,. \tag{10}$$

The right-hand side of Eq. (10) is similar to the following expression:

$$w_i \left(1 + \frac{c_i}{c_s^2}\left(\frac{\tau F_a}{\rho} + u_\alpha\right) + \frac{Q_{i\alpha\beta}}{2c_s^4}\left(\frac{\tau F_\alpha}{\rho} + u_\alpha\right)\left(\frac{\tau F_\beta}{\rho} + u_\beta\right)\right). \tag{11}$$

As a result, the flow velocity can be redefined as $\mathbf{u} \to \mathbf{u} + \mathbf{F}\tau/\rho$. This way, virtually any (soft-core) force term can be incorporated within the equilibrium function (of course, stability can be compromised by large values of the force shifts, which is the reason why the SC formulation cannot sustain very large density contrasts). It is worth pointing out that the additional term, $\tau^2 F_\alpha F_\beta/\rho^2$, in the equilibrium function represents a higher order contribution, which can be tracked to a diffusion term in velocity space, of the form $D_{\alpha\beta}\partial f/\partial_{v_\alpha}\partial_{v_\beta}$, with $D_{\alpha\beta} = 1/2F_\alpha F_\beta \tau^2$. This shows that the Shan–Chen formulation of multiphase flows derives from a Lattice Boltzmann–Fokker–Planck continuum kinetic equation. This is only natural, since the Shan–Chen forcing term corresponds to a soft-core interaction, produces smooth changes of the particle velocities, as opposed to the hard-core, sudden changes described by the Boltzmann collision operator, be it in BGK or MRT form. In passing, we note that by a proper choice of the collisional spectrum, the LB in matrix form can indeed describe the lattice implementations of the Fokker–Planck equations.[27]

2. Shan–Chen Model

In Shan–Chen model,[10] the force at a given node depends on all local neighbours characteristics:

$$\mathbf{F} = G\psi_0 \sum_i w_i \psi_i \mathbf{c_i}\,, \tag{12}$$

where ψ is the function of local characteristics of node. In the above, ψ_0 denotes the local value at a given lattice site, and the summation, i, is taken over neighbors of the node defined by the discrete speed $\mathbf{c_i}$.

2.1. *Equation of state*

The equation of state for LBE^2 is $P = c_s^2\rho$. However, the inclusion of a density-dependent force term brings about a non-ideal contribution. Upon Taylor expansion, the Shan–Chen force (12) for D2Q9 can be expressed as follows:

$$\begin{aligned}\mathbf{F} = {} & G\psi(x,y)(w_1\psi(x+c\Delta t,y)\mathbf{c_1} + w_2\psi(x,y+c\Delta t)\mathbf{c_2} + w_3\psi(x-c\Delta t,y)\mathbf{c_3} \\ & + w_4\psi(x,y-c\Delta t)\mathbf{c_4} + w_5\psi(x+c\Delta t,y+c\Delta t)\mathbf{c_5} \\ & + w_6\psi(x-c\Delta t,y+c\Delta t)\mathbf{c_6} + w_7\psi(x-c\Delta t,y-c\Delta t)\mathbf{c_7} \\ & + w_8\psi(x+c\Delta t,y-c\Delta t)\mathbf{c_8}) = G\psi\left(\frac{1}{3}\nabla\psi + \frac{1}{18}\nabla\Delta\psi\right),\end{aligned}$$

$$F_\alpha = G\psi\left(c_s^2\partial_\alpha\psi + \frac{c_s^4}{2}\partial_\alpha\Delta\psi\right) = G\left(\frac{c_s^2}{2}\partial_\alpha\psi^2 + \frac{c_s^4}{2}(\partial_\alpha(\psi\Delta\psi) - \Delta\psi\partial_\alpha\psi)\right)$$

$$= G\left(\frac{c_s^2}{2}\partial_\alpha\psi^2 + \frac{c_s^4}{2}\left(\partial_\alpha(\psi\Delta\psi) + \frac{1}{2}\partial_\alpha(\nabla\psi)^2 - \partial_\beta\partial_\alpha\psi\partial_\beta\psi\right)\right). \tag{13}$$

The momentum-flux tensor obeys a conservative equation:[11]

$$\partial_\beta\mathbb{P}_{\alpha\beta} = -F_\alpha + \partial_\alpha(p) = -F_\alpha + \partial_\alpha(c_s^2\rho)\,.$$

Thus, the flux tensor $\mathbb{P}_{\alpha\beta}$ is modified as follows:

$$\mathbb{P}_{\alpha\beta} = \left(c_s^2\rho + G\frac{c_s^2}{2}\psi^2 + G\frac{c_s^4}{2}|\nabla\psi|^2 + G\frac{c_s^2}{2}\psi\Delta\psi\right)\delta_{\alpha\beta} - \frac{c_s^4}{2}\partial_\alpha\psi\partial_\beta\psi$$

and the potential is given by

$$V = G\frac{c_s^2}{2}\psi^2 + G\frac{c_s^4}{2}|\nabla\psi|^2 + G\frac{c_s^4}{2}\psi\Delta\psi\,. \tag{14}$$

Since the gradient terms in Eq. (14) are small compared with the leading terms (the characteristic length of the interface is longer than the lattice spacing, as in all diffuse-interface methods), Eq. (14) can be approximated as

$$p = \rho c_s^2 + G\frac{c_s^2}{2}\psi^2\,. \tag{15}$$

By a suitable choice of the pseudo-potential $\psi(\rho)$, this equation can describe phase-separation. Let us assume that the function ψ depends on ρ only. We can determine G_{crit} and ρ_{crit} from the following equations:

$$\frac{dp}{d\rho} = c_s^2 + Gc_s^2\psi\psi' = 0\,, \tag{16}$$

$$\frac{d^2p}{d\rho^2} = Gc_s^2(\psi\psi'' + (\psi')^2) = 0\,. \tag{17}$$

For the typical choice $\psi(\rho) = 1 - e^{-\rho}$ (see later), this delivers the criticality condition:

$$G < G_{\text{crit}} = -4$$

and $\rho_{\text{crit}} = \ln 2$. Note that negative G corresponds to attractive interactions, the typical case of Shan–Chen applications.

2.2. *2D phase separation*

Let us examine a phase transition in a planar case, with the y coordinate normal to the interface. The gas/vapor phase occupies the upper domain, while a liquid occupies the lower domain. So, there are two boundary conditions: $\rho(\infty) = \rho_g$ and $\rho(-\infty) = \rho_l$. The normal component $\mathbb{P}_{yy}$ to the phase interface should be constant,

because there is no any flux in the y direction. As the pressure is the same in both domains $\mathbb{P}_{yy}(\infty) = \mathbb{P}_{yy}(-\infty)$, then

$$p_0 = c_s^2\rho + \frac{Gc_s^2}{2}\psi(\rho_g)^2 = c_s^2\rho + \frac{Gc_s^2}{2}\psi(\rho_l)^2\,. \tag{18}$$

The condition of constant flux $\mathbb{P}_{yy}$ reads as:

$$p_0 = c_s^2\rho + \frac{Gc_s^2}{2}\psi^2 + \frac{Gc_s^4}{4}(\psi'\rho')^2 + \frac{Gc_s^4}{2}\psi(\psi''\rho'^2 + \psi'\rho'')\,. \tag{19}$$

In the above equation there is no independent variable. In such a situation, the substitution $(\rho')^2 = z$ simplifies it; note that $\rho'' = (d\rho'/d\rho)(d\rho/dy) = (d\sqrt{z}/d\rho)\sqrt{z} = z'/2$. After some algebraic manipulations, the following first-order equation is obtained:

$$z'\frac{Gc_s^4}{4}\psi\psi' + z\frac{Gc_s^4}{4}(2\psi\psi'' - \psi'^2) = p_0 - c_s^2\rho + \frac{Gc_s^2}{2}\psi^2\,.$$

The equation presented in the Sturm–Liouville form, $y' + p(x)y = q(x)$, has the following solution $y = e^{-\int p(x)dx}(\int q(x)e^{\int p(x')dx'dx} + C)$. Therefore,

$$z = \frac{\psi}{\psi'^2}\left(\frac{4}{Gc_s^4}\int\left(p_0 - c_s^2\rho - \frac{Gc_s^2}{2}\psi^2\right)\frac{\psi'}{\psi^2}d\rho + C\right)\,. \tag{20}$$

For Eq. (20) to be consistent with the boundary conditions and to define constant C, we need to impose:

$$\int_{\rho_g}^{\rho_l}\left(p_0 - c_s^2\rho - \frac{Gc_s^2}{2}\psi^2\right)\frac{\psi'}{\psi^2}d\rho = 0\,. \tag{21}$$

The specific form of the pseudo-potential ψ is obtained through the Maxwell equal area reconstruction, from Van der Waals's equation[10] $\int_{\upsilon_l}^{\upsilon_g}(p_0 - p)d\upsilon = 0$, where $\upsilon \approx 1/\rho$. Hence,

$$\int_{\rho_g}^{\rho_l}\left(p_0 - c_s^2\rho - \frac{Gc_s^2}{2}\psi^2\right)\frac{1}{\rho^2}d\rho = 0\,.$$

That means function $\psi(\rho) = 1/C + 1/\rho$. If constant $C = 0$, then $\psi(\rho) = \rho$. This contributes a quadratic term in the equation of state, which would lead to an attractive instability at sufficiently high densities. To tame these instabilities, the function is taken in the following form:

$$\psi(\rho) = \sqrt{\rho_0}\left(1 - \exp\left(-\frac{\rho}{\rho_0}\right)\right)\,. \tag{22}$$

Note that at high densities $\rho > \rho_0$, the potential goes to a constant, and consequently the associated force vanishes, thereby saturating the attractive instability. The exact form of function ψ being available, we can find all unknown values ρ_g, ρ_l from (18)–(21) and also compute the density profile from (20). For the standard form of the function ψ, one can perform simulation and obtain ρ_g and ρ_l dependency on G (Fig. 1).

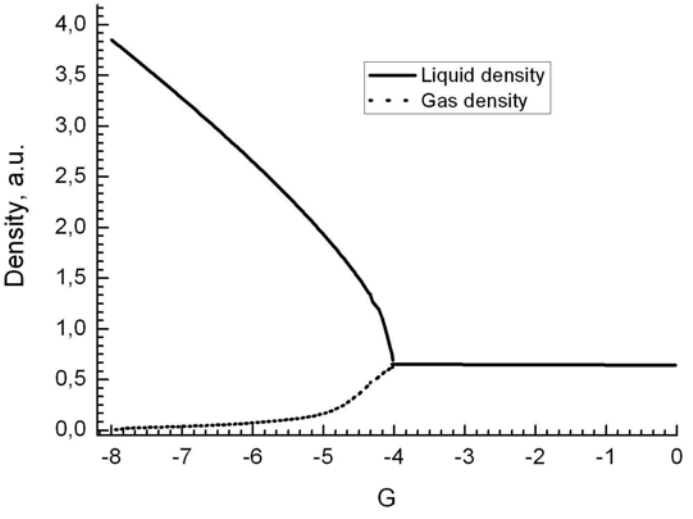

Fig. 1. High and low density dependances on G. Curve obtained from Eqs. (18) and (21). There is no separation until G equals $G_{\text{crit}} = -4$. The initial density was taken $\rho = \rho_{\text{crit}} = \ln 2$.

2.3. *Critical values and σ*

Let us obtain critical values from (16) and (17). For the most popular function (22) one can obtain $G_{\text{crit}} = -4$ and $\rho_{\text{crit}} = \rho_0 \ln 2$. For the function defined as $\psi(\rho) = (1/C + 1/\rho)$ one can obtain that $\rho_{\text{crit}} = 1/2C$ and $G_{\text{crit}} = -27/4C$.

Surface tension is defined as the integral along a flat surface of the mismatch between the normal $\mathbb{P}_{yy}$ and transversal $\mathbb{P}_{xx}$ components of the flux tensor:[11]

$$\sigma = \int_{-\infty}^{+\infty} (\mathbb{P}_{yy} - \mathbb{P}_{xx}) dy = -\frac{G c_s^4}{2} \int_{-\infty}^{+\infty} |\partial_y \psi|^2 dy \,.$$

Note that the surface tension and the equation of state depend on the same parameter G, which is clearly a limitation of the Shan–Chen model.

3. Matrix Representation

There are a few possibilities to represent collision operator, such as BGK,[5] MRT,[14,15,23,28] and TRT[16] representations. In general, the collision operator can be formulated as:

$$\Omega f^{n\,\text{eq}} = \int \Omega(\upsilon, \upsilon', \mathbf{r}, t)(f^{\text{eq}}(\upsilon') - f(\upsilon)) d\upsilon' \,,$$

where

$$\Omega(\upsilon, \upsilon', \mathbf{r}, t) = W(\upsilon) \sum_k H_k(\upsilon) w_k(\mathbf{r}, t) H_k(\upsilon') \,,$$

where H_k is the Hermite's polynomial of kth order. Let us reformulate the collision operator as follows:

$$\Omega f^{n\,\mathrm{eq}} = \sum_j A_{ij}(f_j^{\mathrm{eq}} - f_j)\,.$$

Thus, the LBE takes the form,[15,17]

$$f_i(\mathbf{r} + \mathbf{c_i}\Delta t, c_i, t) - f_i(\mathbf{r}, \mathbf{c_i}, t) = -\sum_j A_{ij}(f_j(\mathbf{r}, \mathbf{c_i}, t) - f_j^{\mathrm{eq}}(\mathbf{r}, \mathbf{c_i}, t))\,. \tag{23}$$

3.1. *Matrix eigenvalues*

The continuity equation can be recovered by summing over all populations of Eq. (23), where the right-hand side of Eq. (23) equals to 0, which means $\sum_{i,j} A_{ij}(f_j^{\mathrm{eq}} - f_j) = 0$ or $\sum_{i,j} A_{ij} = 0$. The matrix A_{ij} has the eigenvalue 0 and eigenvector (1, 1, 1, 1, 1, 1, 1, 1, 1). Hence, the matrix A_{ij} has eigenvectors corresponding to the moments of the Navier–Stokes equations. These properties were discussed in detail by Benzi *et al.*,[29] and later reconsidered by d'Humieres,[14] Ginzburg,[16] Ginzburg and coworkers,[17] Lallemand and Luo[15] and in the moment's space. Therefore, all the moments can be expressed in terms of Hermite'polynomials:

$$\begin{aligned}
|A_\rho\rangle &= (1,1,1,1,1,1,1,1,1)\,,\\
|A_{J_x}\rangle &= (0,1,0,-1,0,1,-1,-1,1)\,,\\
|A_{J_y}\rangle &= (0,0,1,0,-1,1,1,-1,-1)\,,\\
|A_{\mathbb{P}_{xx}}\rangle &= \left(-\frac{1}{3},\frac{2}{3},-\frac{1}{3},\frac{2}{3},-\frac{1}{3},\frac{2}{3},\frac{2}{3},\frac{2}{3},\frac{2}{3}\right)\,,\\
|A_{\mathbb{P}_{xy}}\rangle &= (0,0,0,0,0,1,-1,1,-1)\,,\\
|A_{\mathbb{P}_{yy}}\rangle &= \left(-\frac{1}{3},-\frac{1}{3},\frac{2}{3},-\frac{1}{3},\frac{2}{3},\frac{2}{3},\frac{2}{3},\frac{2}{3},\frac{2}{3}\right)\,,\\
|A_{J_\gamma}\rangle &= (1,-2,-2,-2,-2,4,4,4,4)\,,\\
|A_{J_{\gamma_x}}\rangle &= (0,-2,0,2,0,4,-4,-4,4)\,,\\
|A_{J_{\gamma_y}}\rangle &= (0,0,-2,0,2,4,4,-4,-4)\,,
\end{aligned}$$

where $|\,\rangle$ corresponds to the ket notation. All eigenvectors are constructed from the velocity set, as follows:

$$\begin{aligned}
|A_\rho\rangle &= 1_i\,,\\
|A_{J_x}\rangle &= c_{ix}\,,\\
|A_{J_y}\rangle &= c_{iy}\,,\\
|A_{\mathbb{P}_{xx}}\rangle &= \mathbb{Q}_{xx} = c_{ix}^2 - c_s^2\,,\\
|A_{\mathbb{P}_{xy}}\rangle &= \mathbb{Q}_{xy} = c_{ix}c_{iy}\,,
\end{aligned}$$

$$
\begin{aligned}
|A_{\mathbb{P}_{yy}}\rangle &= \mathbb{Q}_{yy} = c_{iy}^2 - c_s^2\,,\\
|A_{J_\gamma}\rangle &= g_i = 1 - 6(c_i x^2 + c_i y^2) + 3(c_i x^2 + c_i y^2)^2\,,\\
|A_{J_{\gamma_x}}\rangle &= g_i c_{ix}\,,\\
|A_{J_{\gamma_y}}\rangle &= g_i c_{iy}\,.
\end{aligned}
$$

The eigenvectors corresponding to the equilibrium moments of Navier–Stokes equation can be written as

$$
|\rho, J_x, J_y, \mathbb{P}_{xx}, \mathbb{P}_{xy}, \mathbb{P}_{yy}, J_\gamma, J_{\gamma_x}, J_{\gamma_y}\rangle = \rho|1, u_x, u_y, u_x^2, u_x u_y, u_y^2, u_x^2 u_y^2, u_x u_y^2, u_y u_x^2\rangle\,. \tag{24}
$$

Notice that matrix representation above considers all the moments of Navier–Stokes equation, as they can be seen in an equilibrium function (4). Therefore, the matrix representation differs from the matrix presented in the papers.[15,17] To the best of the authors knowledge, this matrix representation is given only in Ref. 28.

By summation over $c_{i\alpha}$, we obtain $\sum A_{ij} c_{j\alpha} = 0 = 0 \cdot c_{i\alpha}$. Therefore, two eigenvectors (c_{ix} and c_{iy}) are noted above. To obtain the proper viscosity term, we need to satisfy the condition $\sum_j A_{ij}\mathbb{Q}_{j\alpha\beta} = w_{\alpha\beta}\mathbb{Q}_{i\alpha\beta}$. Therefore, there is a need for six eigenvectors to restore the Navier–Stokes equations. Three eigenvectors are $A^{(0)} = A_\rho = 1_i$, $A^{(1)} = A_{J_x} = c_{ix}$, $A^{(2)} = A_{J_y} = c_{iy}$, with eigenvalue $\omega_0 = \omega_1 = \omega_2 = 0$, because mass and momentum are conserved by definition and other three eigenvectors $A^{(3)} = A_{\mathbb{P}_{xx}} = \mathbb{Q}_{ixx}$, $A^{(4)} = A_{\mathbb{P}_{xy}} = \mathbb{Q}_{ixy}$, $A^{(5)} = A_{\mathbb{P}_{yy}} = \mathbb{Q}_{iyy}$ with eigenvalues $\omega_3 = w_{xx}$, $\omega_4 = w_{xy}$, $\omega_5 = w_{yy}$, corresponding to the momentum flux, which is not microscopically conserved.

The remaining three eigenvectors identify with Hermite polynomials in the velocity space, which are orthogonal to all other six eigenvectors. From here on, the eigenvalues are denoted by $\omega_6 = \gamma$, $\omega_7 = \gamma_x$, $\omega_8 = \gamma_y$.

Also notice that $\sum f_i^{\text{eq}} J_{\gamma_i} = 0$. The analysis is considered in real configuration space, not in the momentum space. This means that the equilibrium function is not changed, but only the collision operator is modified. The eigenvalues γ, γ_x, and γ_y can be tuned to improve the stability of LBM. The three eigenvalues γ, γ_x, and γ_y are called ghost eigenvalues because they are needed for symmetry reasons, although they do not surface to the Navier–Stokes equation.[29] A discussion on the way that the eigenvectors can be used to restore the matrix A_{ij} is given in the next section.

3.2. *Eigenvectors decomposition*

Any matrix V can be represented in the so-called *spectral representation* $V_{ij} = \sum_k V_i^{(k)} \omega_k V_j^{(k)}$, where ω_k are eigenvalues and $V^{(k)}$ are eigenvectors, and $\sum_i V_i^{(j)} V_i^{(k)} = \delta_{jk}$ is an orthogonality condition. Also, the matrix A_{ij} can be decomposed as:

$$A_{ij} = w_i \sum_k A_i^{(k)} \omega_k A_j^{(k)} , \tag{25}$$

where w_i are the weights defined in (5).

Please note that Eq. (25) is weighted by w_i. This is because the orthogonality conditions are slightly different, namely

$$\sum_k w_i A_i^{(k)} A_j^{(k)} = \delta_{ij} ,$$

$$\sum_i w_i A_i^{(j)} A_i^{(k)} = \delta_{jk} .$$

For all these transformations, the following formula is introduced:

$$F_k = \sum_i f_i A_i^{(k)} , \tag{26}$$

where F_k are the kinetic moments from Eq. (24). However, the inverse formula explicitly includes the weights:

$$f_i = w_i \sum_i F_k A_i^{(k)} . \tag{27}$$

To insure that Eqs. (26) and (27) are consistent:

$$f_i = w_i \sum_k F_k A_i^{(k)} = w_i \sum_k \sum_j f_j A_j^{(k)} A_i^{(k)}$$

$$= \sum_j f_j \sum_k w_i A_j^{(k)} A_i^{(k)} = \sum_j f_j \delta_{ij} = f_i .$$

Note that for BGK, all eigenvalues equal $\omega = 1/\tau$. For this case, from the orthogonality of the eigenvectors, it follows that:

$$A_{ij} = w_i \sum_k A_i^{(k)} \omega_k A_j^{(k)} = \omega \sum_k A_i^{(k)} w_i A_j^{(k)} = \omega \delta_{ij} .$$

The collision operator can then be written in terms of eigenvectors, eigenvalues, and kinetic moments equation as follows:

$$\begin{aligned}
\sum_j A_{ij}(f_j - f_j^{\mathrm{eq}}) &= \sum_j (f_j - f_j^{\mathrm{eq}}) w_i \sum_k A_i^{(k)} \omega_k A_j^{(k)} \\
&= \sum_k w_i A_i^{(k)} \omega_k \sum_j (f_j - f_j^{\mathrm{eq}}) A_j^{(k)} = \sum_k w_i A_i^{(k)} \omega_k (F_k - F_k^{\mathrm{eq}}) \\
&= w_i(\omega_0 1_i(\rho - \rho^{\mathrm{eq}}) + \omega_1 c_{ix}(J_x - J_x^{\mathrm{eq}}) + \omega_2 c_{iy}(J_y - J_y^{\mathrm{eq}}) \\
&\quad + \omega_3 \mathbb{Q}_{ixx}(\mathbb{P}_{xx} - \mathbb{P}_{xx}^{\mathrm{eq}}) + \omega_4 \mathbb{Q}_{ixy}(\mathbb{P}_{xy} - \mathbb{P}_{xy}^{\mathrm{eq}}) + \omega_5 \mathbb{Q}_{iyy}(\mathbb{P}_{yy} - \mathbb{P}_{yy}^{\mathrm{eq}}) \\
&\quad + \omega_6 g_i (J_\gamma - J_\gamma^{\mathrm{eq}}) + \omega_7 g_i c_{ix}(J_{\gamma_x} - J_{\gamma_x}^{\mathrm{eq}}) + \omega_8 g_i c_{iy}(J_{\gamma_y} - J_{\gamma_y}^{\mathrm{eq}})) .
\end{aligned} \tag{28}$$

As far as the first three eigenvalues are equal to 0, the equilibrium distribution function can be modified so as to carry its own independent density and current, that is $\rho \neq \rho^{\mathrm{eq}}$ and $J \neq J^{\mathrm{eq}}$.

It should be mentioned that usually the eigenvalues corresponding to the density and flux momentum are taken 0 and equilibrium functions equal to exact conserved moments.

3.3. *Force incorporation within the matrix collision operator*

Let us recall that force and equilibrium distribution function are represented in a series of moments of the Boltzmann equation. The source term associated with the force can be reconstructed in a similar way:

$$S_i = w_i \sum_k s_k A_i^k = w_i(s_0 1_i + s_1 c_{ix} + s_2 c_{iy} + s_3 \mathbb{Q}_{ixx} + s_4 \mathbb{Q}_{ixy} + s_5 \mathbb{Q}_{iyy} + s_6 g_i + s_7 g_i c_{ix} + s_8 g_i c_{iy}),$$

where s_k are the moments of the force. To be consistent with a restoration of force term in a Navier–Stokes equation, the above expression turns to be:

$$S_i = w_i \left(\frac{F_{i\alpha} c_{i\alpha}}{c_s^2} + \rho \frac{F_\alpha u_\beta + F_\beta u_\alpha}{2c_s^4} [c_{i\alpha} c_{i\beta} - c_s^2 \delta_{\alpha\beta}] + s_6 g_i + s_7 g_{ix} + s_8 g_{iy} \right).$$

Then the force term can be incorporated in the equilibrium function, the same way it was done with BGK collision operator representation. For this purpose, the equation below has to be solved:

$$-\sum_j A_{ij}(f_j - f_j^{\mathrm{eq}}) = -\sum_j A_{ij}(f_j - \widetilde{f_j^{\mathrm{eq}}}) + S_i \,. \tag{29}$$

We can obtain $\widetilde{f_i^{\mathrm{eq}}}$ from the equation above as:

$$\widetilde{f^{\mathrm{eq}}} = f^{\mathrm{eq}} - A^{-1} S \,.$$

Clearly, if the matrix A has zero eigenvalues, this expression is not defined (A^{-1} is a pseudo-inverse). This formal problem can be circumvented as follows. Let us write the change in the population f_i due to collisions and force term as follows:

$$C_i = \sum_j A_{ij}(f_j^{\mathrm{eq}} - f_j) + S_i = w_i \sum_k \omega_k (F_k^{\mathrm{eq}} - F + s_k) A_i^k \,.$$

This expression shows that by choosing $\omega_{0,1,2} \neq 0$, like in BGK, mass and momentum conservation impose the conditions $\rho^{\mathrm{eq}} = \rho$, $J^{\mathrm{eq}} = J$ and s_0 can be any value. On the other hand, with $\omega_0 = 0$, one is free to choose $\rho^{\mathrm{eq}} \neq \rho$, provided $s_0 = 0$. This shows that the matrix formulations leave more freedom on the local equilibrium, and particular on the equilibrium density. As we shall see, this freedom on the conserved quantities helps reducing finite-compressibility errors.

For the non-conserved ones, the idea is to give ghost their own relaxation time, independent of the one of the momentum flux tensor. As we shall see, this helps the numerical stability of the method in the low-viscosity regime.

An example of an equilibrium functions satisfying the above requests $\rho \neq \rho^{\mathrm{eq}}$ is the following:

$$f_i^{\mathrm{eq}} = w_i \left(\rho_0 + \rho \frac{c_{i\alpha} u_\alpha}{c_s^2} + \cdots \right) .$$

If all eigenvalues are non-zero, then $\tilde{f}^{\mathrm{eq}}$ will be defined as:

$$\tilde{f}_i^{\mathrm{eq}} = w_i \Bigg(1 + \frac{c_{i\alpha}(u_\alpha + F_\alpha/\omega_\alpha)}{c_s^2} + \frac{\mathbb{Q}_{i\alpha\beta}}{2c_s^4} \left(u_\alpha - \frac{F_\alpha}{\omega_{\alpha\beta}} \right) \left(u_\beta - \frac{F_\beta}{\omega_{\alpha\beta}} \right) + \tilde{s}_6 g_i + \tilde{s}_7 g_i c_{ix} + \tilde{s}_8 c_{iy} \Bigg) , \tag{30}$$

where $\omega_\alpha = \omega_{1,2}$, $\omega_{\alpha\beta} = \omega_{3,4,5}$, $\tilde{s}_{6,7,8} = s_{6,7,8} + J^{\mathrm{eq}}_{\gamma_{x,y}}$. Note that Eq. (29) is not the only way to invert the collision matrix. One can try to solve the equation below for the two unknowns $\widetilde{f^{\mathrm{eq}}}$ and $\tilde{A}_{ij}$:

$$-\sum_j \tilde{A}_{ij}(f_j - f_j^{\mathrm{eq}}) = -\sum_j A_{ij}(f_j - \widetilde{f_j^{\mathrm{eq}}}) + S_i .$$

After matrix inversion, one obtains

$$\widetilde{f^{\mathrm{eq}}} = \tilde{A}^{-1} A (f^{\mathrm{eq}} - f) + \tilde{A}^{-1} S .$$

To the best of our knowledge, this route does not appear to have been explored to date.

4. Numerical Results

4.1. *Droplet simulation*

To illustrate the validity of the previous analysis a droplet formation is simulated. A square domain with periodical boundary conditions sized 128 on 128 nodes is considered. A droplet is placed in the center with $\rho_l = 2.8$ and radius $R = 20$ in lattice units. The remaining domain is filled with density $\rho_{\mathrm{gas}} = 0.05$. For comparison purposes, simulations with BGK collision operator are first carried out.

4.1.1. *BGK instability in droplet formation*

The gas-liquid density ratio is controlled by the parameter G (a sort of inverse temperature), as shown in Fig. 1. However, Shan–Chen droplet simulation with BGK collision operator is limited to a given value of G, corresponding to liquid-gas density ratios no greater than 60–80.

The instability appears in the form of spurious currents around the droplet (Fig. 2).[11] These spurious currents are also presented as a vector field around the droplet, Fig. 3. For the sake of simplicity, a droplet of radius $R = 10$ units is considered. For this value of R, the quadrupole structure of spurious currents is

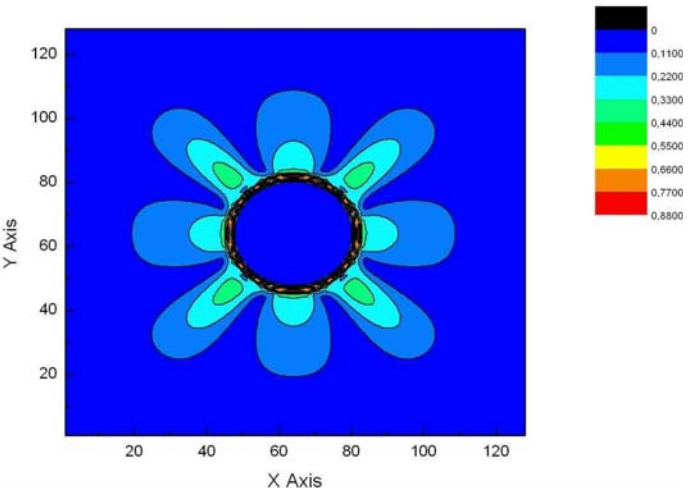

Fig. 2. Spurious currents around the droplet. Here it is taken Mach number $\sqrt{(u_x^2 + u_y^2)}/c_s$ to show spurious currents.

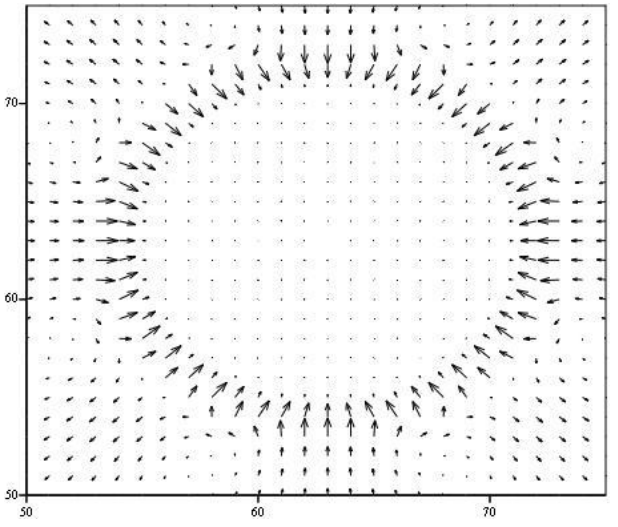

Fig. 3. Vector field of currents around droplet. One can see that structure of velocities is quadrupole.

well visible. The spurious currents can be analyzed through a Taylor expansion of the Shan–Chen force:[11]

$$c_s^2 \sum_i w_i \psi(\mathbf{x} + \mathbf{c}_i \Delta t)\mathbf{c}_i = \nabla \left(1 + \frac{1}{6}\nabla^2 + \frac{1}{72}\nabla^2\nabla^2\right)\psi + \mathbf{e}_x \frac{\partial_x^5 \psi}{180} + \mathbf{e}_y \frac{\partial_y^5 \psi}{180}\,. \quad (31)$$

The discussion of the mechanism by which this instability progresses in time will be presented in the next section. Simulation, Fig. 4, shows that the instabilities

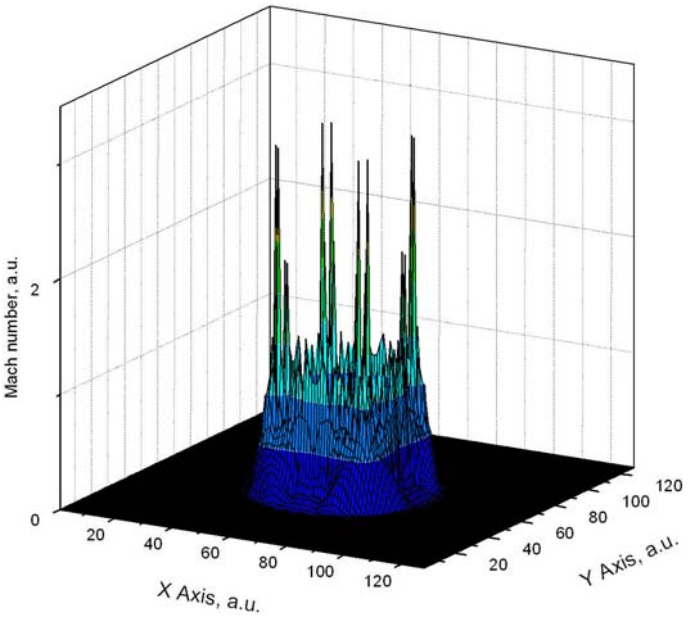

Fig. 4. Mach number around the droplet just before instability occurs (2D profile). One can see the quadrupole structure.

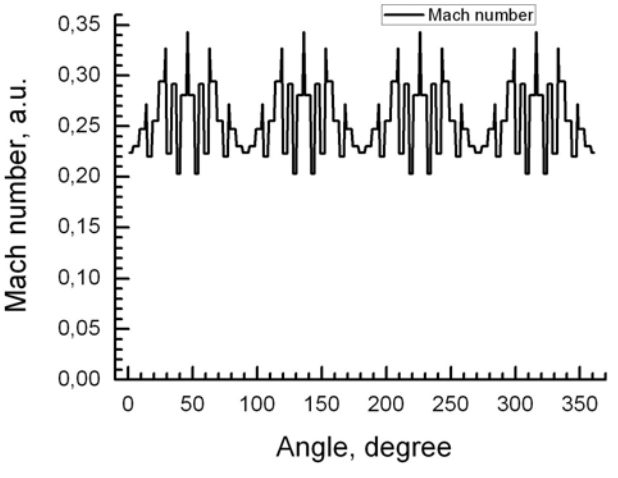

Fig. 5. Angle Mach number profile on $R = 20$. The same as in Fig. 4.

appear at the interface in the form of peaks in the local Mach number. These peaks are related to anisotropic components of the Shan–Chen force, as evidenced by the quadrupole structure of the peaks in Fig. 5, showing Mach number dependency on angle with fixed radius $R = 20$. In the following section, we discuss the parameters that infuence the progress of this instability.

4.1.2. *Parameters*

The instability progress and the maximum critical value of G are influenced by a number of parameters, such as the initial liquid density ρ_l, gas density ρ_g, and the droplet radius R. For example, if initial conditions are chosen as $\rho_l = 1.01\ln 2$ and $\rho_g = 0.99\ln 2$, for a droplet with $R = 40$, the instability will occur for $G = -6.33$ with BGK collision operator. However, by taking $\rho_l = 2.8$ and $\rho_g = 0.05$ with the same radius, the instability occurs at $G = -8.4$. The critical G at which the system becomes unstable, also increases as the radius decreases. That means that the cause of instability is the momentum-flux tensor, $\mathbb{P}_{ij}$, whose divergence gives the force term. Clearly, the flux tensor is sensitive to the "distance" of the initial condition from the steady-state one, as well as to the droplet radius. It is, therefore, natural that the instability can be softened by choosing initial conditions close to the steady-state ones. Hence, it is possible to use large G values, in combination with proper values of the radius and initial droplet and media densities.

The results of using MRT model will be described in the following section.

4.1.3. *Matrix collision operator*

In the simulations, the equilibrium function (30) is taken without ghost contributions, i.e., $\tilde{s}_{6,7,8} = 0$, with truncated equilibra. Also we considered a shifted equilibrium function (11) with only one value 1.0, therefore all kinetic moments are redefined in terms of the shifted velocities (central moments):

$$|\tilde{F}\rangle = \rho|1, v_x + u_x, v_y + u_y, (v_x + u_x)(v_x + u_x), (v_x + u_x)(v_y + u_y), (v_y + u_y)$$
$$(v_y + u_y), (v_x + u_x)^2(v_y + u_y)^2, (v_x + u_x)(v_y + u_y)^2, (v_y + u_y)(v_x + u_x)^2\rangle\,,$$

where $\mathbf{u} = \mathbf{F}\tau/\rho$ is a shift due to Shan–Chen force, where $\tau = 1.0$. Let us recall the equilibrium function with a Shan–Chen force incorporation (11) for BGK collision operator:

$$f_i^{\mathrm{eq}} = w_i\rho\left(1 + \frac{c_i}{c_s^2}\left(\mathbf{u} + \frac{\mathbf{F}\tau}{\rho}\right) + \frac{\mathbb{Q}_{i\alpha\beta}}{2c_s^4}\left(u_\alpha + \frac{F_\alpha\tau}{\rho}\right)\left(u_\beta + \frac{F_\beta\tau}{\rho}\right)\right).$$

The cause of spurious currents in BGK are the terms $\mathbf{u}+\frac{\mathbf{F}\tau}{\rho}$ and $(u_\alpha+F_\alpha\tau/\rho)(u_\beta+F_\beta\tau/\rho)$. It is known from the simulations with BGK collision operator that these terms cannot be compensated by moments of the external source. However, by inspecting the structure of non-conserved ghost moments, which are actually close to the equilibrium moments $F_7 = \rho(u_x + F_x\tau/\rho)^2(u_y + F_y\tau/\rho)^2$, $F_8 = \rho(u_x + F_x\tau/\rho)(u_y+F_y\tau/\rho)^2$, $F_9 = \rho(u_y+F_y\tau/\rho)(u_x+F_x\tau/\rho)^2$, we realize that these terms have the same structure as those which cause the instability and those terms are present in the collision part of the LBE. Note that the equilibrium ghost moments are equal to 0, as far as the truncated equilibrium distribution function is considered. However, for the non-equilbrium ghost moments the truncated equilibrium function is not considered and by using low-Knudsen approximation one can obtain the ghost moments close to the equilibrium ghost moments in the case of non-truncated

equilibrium distribution function. As a result, within the MRT formulation, ghosts can be used to mitigate the instabilities caused by spurious currents.

As a first approximation, let $f = (1+D\tau)f^{\mathrm{eq}}$, where D is the streaming operator. In that case noticing that the last three eigenvalues are taken equal to each other, i.e., $\omega_{\gamma,\gamma_x,\gamma_y} = \omega_\gamma$ the equilibrium part of the collision operator is examined as

$$\begin{aligned}
&\rho c_{ix,y}\omega_{x,y}\left(u_{x,y}+\frac{F_{x,y}\tau}{\rho}\right)+\omega_{3,4,5}\mathbb{Q}_{i\alpha\beta}\rho\left(u_\alpha+\frac{F_\alpha\tau}{\rho}\right)\left(u_\beta+\frac{F_\beta\tau}{\rho}\right)\\
&\quad+\omega_\gamma g_i\rho\left(u_\alpha+\frac{F_\alpha\tau}{\rho}\right)^2\left(u_\beta+\frac{F_\beta\tau}{\rho}\right)^2\\
&\quad+\omega_\gamma g_i c_{ix}\rho\left(u_\alpha+\frac{F_\alpha\tau}{\rho}\right)\left(u_\beta+\frac{F_\beta\tau}{\rho}\right)^2\\
&\quad+\omega_\gamma g_i c_{iy}\rho\left(u_\alpha+\frac{F_\alpha\tau}{\rho}\right)^2\left(u_\beta+\frac{F_\beta\tau}{\rho}\right).
\end{aligned}$$

By combining all terms containing force terms, the structure of the collision operator can be obtained:

$$\begin{aligned}
&F_x\tau\left(-\omega_x c_{ix}-2\omega_{xx}\mathbb{Q}_{ixx}u_x-2\omega_\gamma g_i\frac{u_x u_y^2}{\rho}-\omega_\gamma g_i c_{ix}\frac{u_y^2}{\rho}-2\omega_\gamma g_i c_{iy}\frac{u_x u_y}{\rho}\right)\\
&\quad+F_y\tau\left(-\omega_y c_{iy}-2\omega_{yy}\mathbb{Q}_{iyy}u_y-2\omega_\gamma g_i\frac{u_x^2 u_y}{\rho}-2\omega_\gamma g_i c_{ix}\frac{u_y u_x}{\rho}-\omega_\gamma g_i c_{iy}\frac{u_x^2}{\rho}\right)\\
&\quad+F_x F_y\tau^2\left(2\omega_{xy}\frac{\mathbb{Q}_{ixy}}{\rho}+4\omega_\gamma g_i\frac{u_x u_y}{\rho^2}+2\omega_\gamma g_i c_{ix}\frac{u_y}{\rho}+2\omega_\gamma g_i c_{iy}\frac{u_x}{\rho}\right)\\
&\quad+F_x^2\tau^2\left(2\omega_{xx}\frac{\mathbb{Q}_{ixy}}{\rho}+\omega_\gamma g_i\frac{u_y^2}{\rho}+\omega_\gamma g_i c_{iy}\frac{u_y}{\rho}\right)\\
&\quad+F_y^2\tau^2\left(2\omega_{yy}\frac{\mathbb{Q}_{iyy}}{\rho}+\omega_\gamma g_i\frac{u_x^2}{\rho}+\omega_\gamma g_i c_{ix}\frac{u_x}{\rho}\right)+\omega_\gamma g_i\frac{F_x^2F_y^2\tau^4}{\rho^4}\\
&\quad+\frac{F_x F_y^2\tau^3}{\rho^3}\left(-2\omega_\gamma g_i u_x-\omega_\gamma g_i c_{ix}\right)+\frac{F_x^2F_y\tau^3}{\rho^3}(-2\omega_\gamma g_i u_y-\omega_\gamma g_i c_{iy})
\end{aligned}\tag{32}$$

Most coefficients of Eq. (32), related to BGK (F_x, F_y, F_xF_y, F_x^2, F_y^2), are negative. However, in the ghost terms these coefficients are positive. Considering that F_x, F_y have quadrupole structure, all combination $F_x^nF_y^m$ will have a higher degree than quadrupole, on top of quadrupole structure itself. Hence, there is a chance that these terms somehow compensate each other.

By tuning all eigenvalues corresponding to ghost currents, the instability of the simulation can be reduced. To show that terms can cancel each other, we numerically investigated the collision operator at each time-step. The collision operator

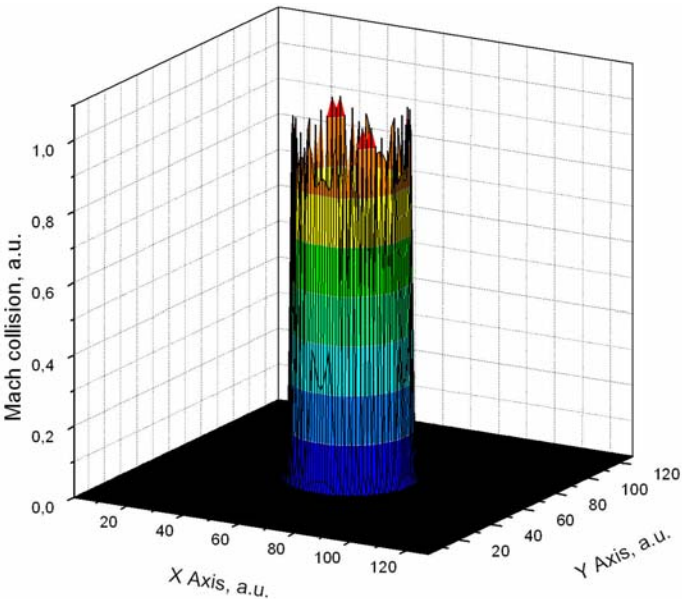

Fig. 6. Mach number for matrix version of collision operator.

for each node and all populations were calculated. The local Mach number for collision operator is defined as $Ma = \sqrt{\delta\rho u_x^2 + \delta\rho u_y^2}/c_s$, where $\delta\rho u_\alpha = \sum_i \delta f_i c_{i\alpha}$. In the above, δf_i represents the effect of the collision operator on f_i in a single time-step. For comparison purpose, the Mach number for collision operator for matrix version and BGK collision operator were constructed. The initial conditions were taken as follows; $\rho_g = 0.05$, $\rho_l = 2.8$, $G = -8.4$. After 1000 iterations, the results of simulation were compared.

Figures 6–9 show Mach number for collision operator after 10 iterations.

It is evident that the results provided by the matrix collision operator exhibit a different structure than the quadrupole BGK collision operator structure. Figures 7 and 9 show variation of Mach number as a function of angle on a radius, $R = 20$. It can be seen that the results of matrix simulation are clearly more isotropic as compared with BGK simulation results. Also, the mean value of the mach number for the BGK collision operator is larger than that of the matrix version ($0.722 > 0.721$) and the standard deviation for BGK collision operator is bigger also ($0.243 > 0.233$). Therefore, simulations lend support to the proposed idea about cancellation of force terms by ghost currents. To further verify this assumption, a few examples were simulated. A droplet simulated with BGK collision operator, with $R = 20$, periodical boundary conditions on a 128×128 domain and initial densities $\rho_l = 2.8$ and $\rho_g = 0.05$, was found to survive instability up to $G = -8.4$. However, with the matrix collision operator stability was preserved up to $G = -8.9$. For $G = -8.5$, ghost eigenvalues $w_\gamma = w_{6,7,8}$ lie in the range 0.6–0.95, while for $G = -8.6$ these

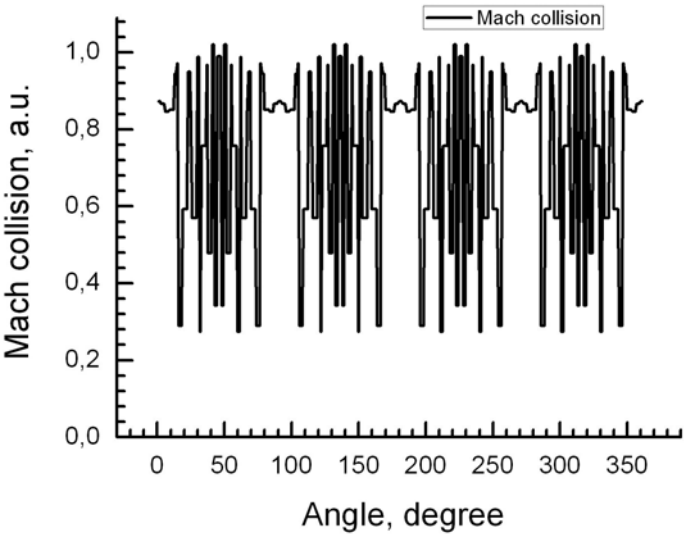

Fig. 7. Mach number for matrix version of collision operator. Line version.

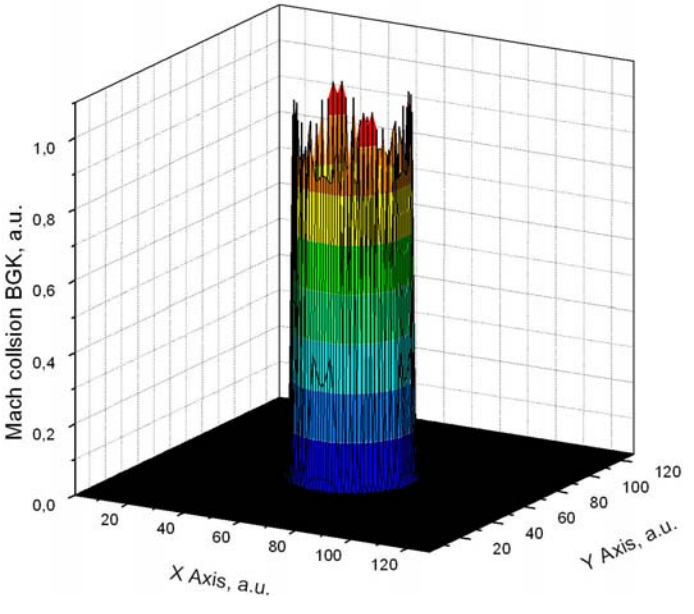

Fig. 8. Mach number for BGK version of collision operator.

values take values in the range $w_\gamma = 0.65$–0.85, and for $G = -8.7$ the range is $w_\gamma = 0.7$–0.75, for $G = -8.8$ values $w_\gamma = 0.71$–0.73. This means that there is a spectral window of ghost eigenvalues which improves the stability of the Shan–Chen model. However, this spectral window shrinks down as G increases. It should be mentioned

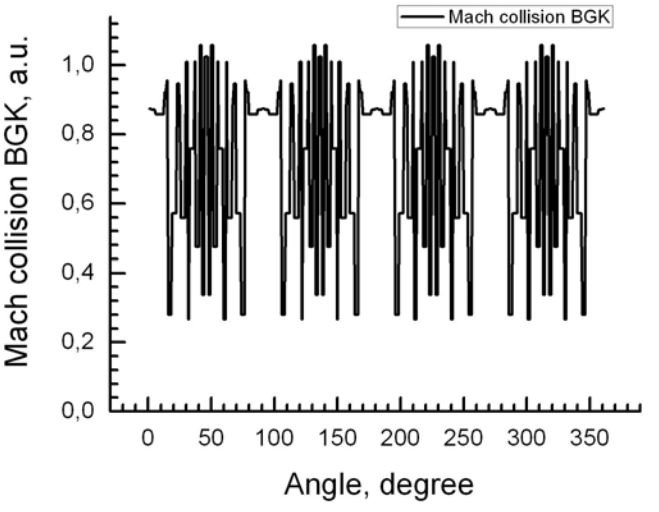

Fig. 9. Mach number for BGK version of collision operator. Line version.

that the window also depends on the droplet radius and initial density conditions, i.e., for radius $R = 3$ and initial values $\rho_l = 5.972$, $\rho_g = 0.05$, one can obtain $G = -12$ with $w_\gamma = 0.915$. Note that all the leading eigenvalues corresponding to the density, momentum, and momentum-flux eigenvalues take a value of unity. Therefore, the stability is achieved by making the lifetime of ghosts longer than that they correlate to the cancellation of the terms ignating instability. Also in the simulations, we switched off all the terms related to the input of force ghost moments to the LBE, i.e., $\tilde{s}_{6,7,8} = 0$ (30). However, by taking them non-zero, a stability enhancement may also obtained.

The bottomline of this section is that the MRT collision operator with equilibrium shifted velocity permits improving the stability of multiphase flow simulation by proper tuning of the ghost eigenvalues. The improvement is shown for the case of droplet simulations. In the next section, we summarize the results obtained for the case of plane interfaces.

4.2. *Plane interface*

Numerical experiments were also performed for plane phase transition, as described by Eq. (18). The purpose is to increase G value, where the scheme breaks down. However, the simulations did not show any dependence of the spurious currents on ghosts eigenvalue ω_γ, Fig. 10. Also, Fig. 10 shows that there is a slight difference between the predicted (20) and numerical results.

These results are in line with the fact that for the Shan–Chen model, spurious currents are only observed in the presence of interface curvature. In the next section, we describe capillary waves simulation results, which have been chosen because capillary waves are naturally affected by the interface curvature.

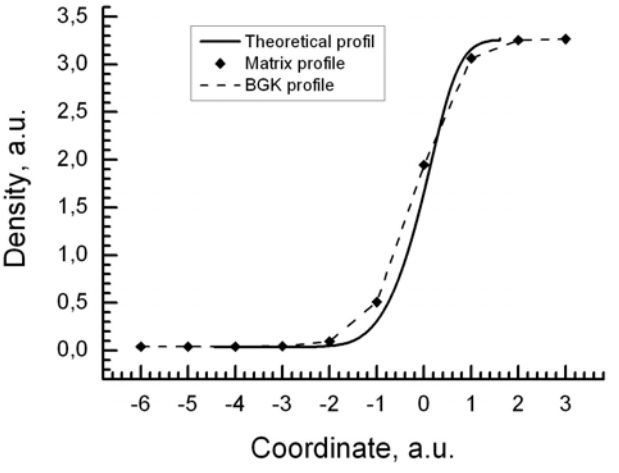

Fig. 10. Calculated theoretical and simulation profiles for $G = -7.0$. For ghost values $\omega_\gamma = 1.5$. However, the ghost profile does not depend on ghost eigenvalue and is always the same as BGK profile.

4.2.1. *Capillary waves*

Capillary waves are well described by Landau and Lifshitz.[30] A small-amplitude, long-wavelength sinusoidal wave is imposed on the interface region. The decay-propagation dynamics of these perturbations are governed by the following dispersion relations

$$\omega^2 = \frac{\sigma}{\rho} k^3 \tag{33}$$

with a decay coefficient, $\gamma = 2\nu k^2$.

The simulations were performed on rectangular domain of 64×256 units, with periodic boundary condition, and without gravity. Let us remind that there are two different ways to impose a sinusoidal wave on the interface. First, a steady-state condition of plane interface problem should be obtained. At steady state, a kink-like density profile across the phase interface is established, and this profile is then subject to a sinusoidal perturbation. The G value should be taken large enough to obtain a sharp density profile. Another possibility is to take steady-state values of gas (ρ_g) and liquid (ρ_l) densities from Eq. (18) and impose sinusoidal wave with sharp gas-liquid interface correspondingly. The difference between two methods is the natural interphase profile obtained in the first method compared with a sharp interface in the second.

Both ways lead to numerical errors, due to imposing density profile not related to the exact solution for capillary waves interface. During simulations additional ripples can occur in the liquid domain which eventually influence on the phase interface. One can see the presence of the ripples at the picture as two stripes in the liquid phase (Fig. 11). Figure 12 shows the density profile crossection.

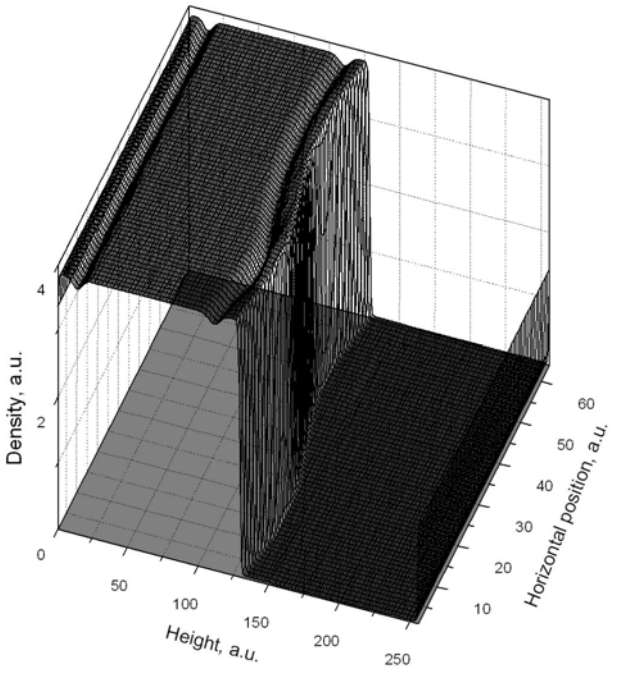

Fig. 11. Capillary waves density profile with numerical error caused by sharp interface between phases.

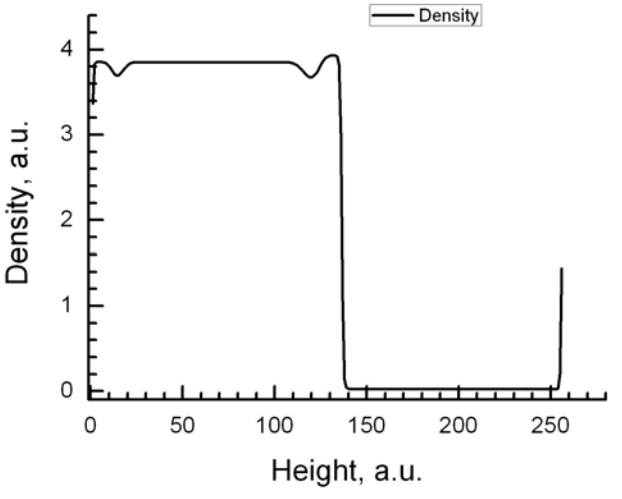

Fig. 12. Crossection for density profile for $y = 20$.

The dispersion relation for capillary waves (33) was examined by Shan and Chen,[10] and McCracken and Abraham.[23] The amplitude for decaying capillary waves with $G = -8.0$ is shown on the Fig. 13.

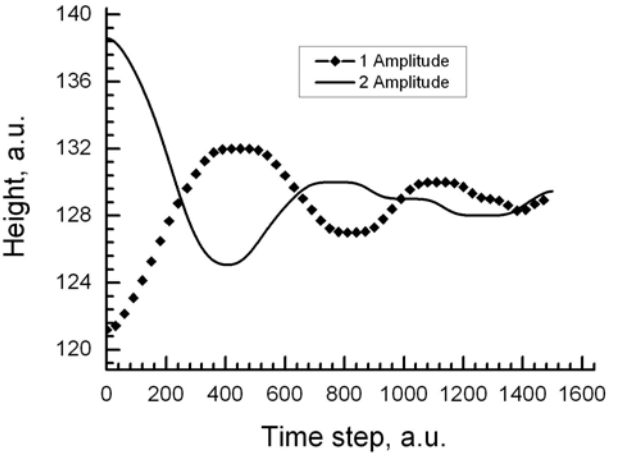

Fig. 13. Amplitude of a capillary wave in time. We took $G = -8.0$ in domain 64 on 256 and initialized domain by $\rho_l = 3.851$ and $\rho_g = 0.0215$.

McCracken and Abraham[23] claimed that the matrix collision operator can bring the limit of low viscosity of multiphase model below the Shan–Chen value.

To further explore this point, we have performed the same numerical experiment. The numerical simulation with BGK collision operator blows up when $\omega > 1.07$. However, with matrix collision operator, $w_{4,5,6} = 1.36$ can be achieved, with $\omega_\gamma = \omega_{6,7,8}$ from 0.75 to 0.92. This result corresponds to 85% improvement. Actually, the performed simulations changes force moments $s_{4,5,6}$, as far as we fixed τ corresponding to the shifted velocity to 1. With conserved moments one can obtain slightly improvement by 8% with $\omega_{\gamma,\gamma_x,\gamma_y} = 0.9$. The eligibility to use such assumption is up to disscussion. However, the Laplace test showed that there is no significant difference to use the assumption. This confirms that the matrix version of collision operator for Shan–Chen model can improve viscosity limit for capillary waves.

4.2.2. *Low viscosity limit*

As matrix version of collision operator improved the low-viscosity limit for capillary waves, let us perform the same simulations for the plane interface. The BGK collision operator can simulate a plane interface phase transition up to $\omega = 1/\tau = 1.08$. Figures 14 and 15 present the instability density profile and crossection correspondingly. Figures 16 and 17 show the instability Mach number with crossection. However, we tried to improve the scheme by matrix collision operator and obtained that the same window for ghost eigenvalues 0.75–0.92 can help to improve the scheme up to $\omega_{3,4,5} = 1.52$ did not show any improvement. However, with proper view of force moments there is no improvement. That supports the idea about ghost currents having a radial structure.

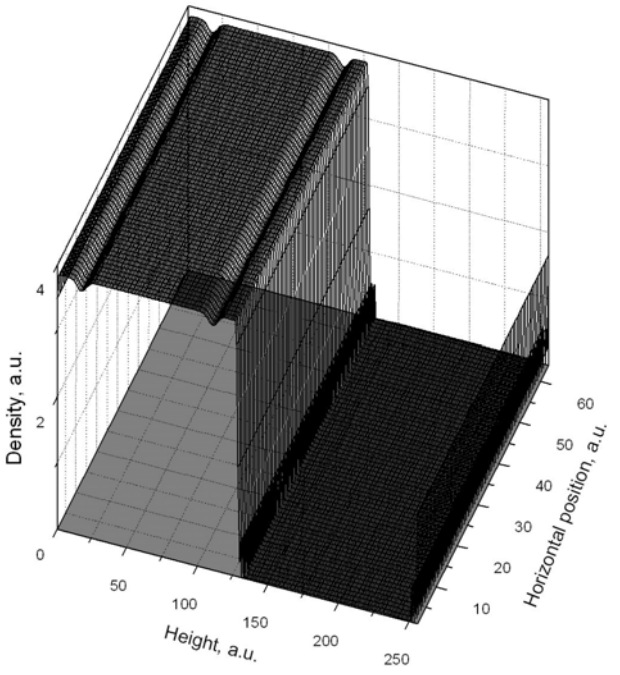

Fig. 14. Instability density profile for plane interface.

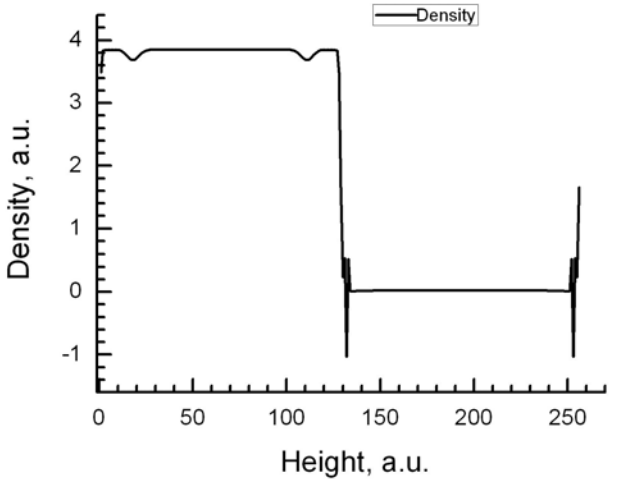

Fig. 15. Density profile middle crossection.

5. Conclusions

Summarizing, the present work shows that by proper tuning of the ghost eigenvalues, the multi-relaxation time collision operator achieves a significant improvement

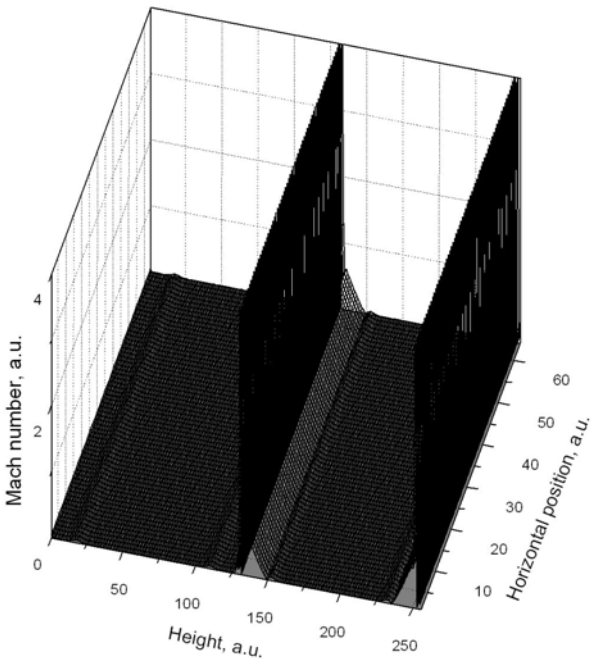

Fig. 16. Mach number for instability plane interface phase separation.

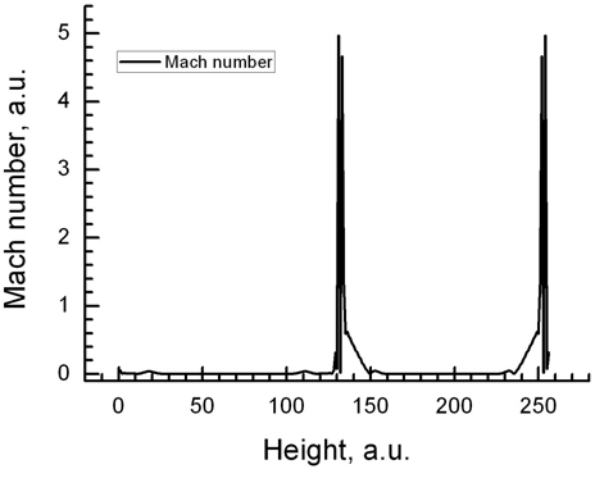

Fig. 17. Mach number middle crossection profile.

in the stability of multiphase flows as compared to the BGK collision operator. In particular, higher density contrasts and lower viscosity regimes for capillary waves can be attained. Many open questions remain to be explored — recovery of hydrodynamic equations through a Chapman–Enskog procedure and extensions

thereof, linear stability analysis and the ensuing prediction of ghost eigenvalues ensuring better stability, as well as optimized local equilibrium functions. Apart from numerical issues, the MRT collision operator will permit the investigation of an entirely new class of multiphase flow phenomena involving non-isotropic fluids with directional viscosity and undergoing non-isotropic phase-transitions driven by directional interactions. This should be of great interest for many applications in chemical engineering and biology.

Acknowledgments

The author (A. Kuzmin) wants to thank Alberta Ingenuity Fund for their financial support. Also the authors would like to thank Dr. M. Sbragaglia for constructive discussion and Dr. I. Ginzburg for the insightful communication. SS wishes to acknowledge financial support from the Killam Foundation, as well as kind hospitality from the Mechanical and Manufacturing Engineering Department at the University of Calgary.

References

1. A. A. Mohamad, *Applied Lattice Boltzmann Method for Transport Phenomena, Momentum, Heat and Mass Transfer* (Sure Print, Calgary, 2007).
2. S. Succi, *The Lattice Boltzmann Equation for Fluid Dynamics and Beyond*, Numerical Mathematics and Scientific Computation (Oxford University Press, Oxford, 2001).
3. M. C. Sukop and D. T. Thorne, *Lattice Boltzmann Modeling An Introduction for Geoscientists and Engineers* (Springer Verlag, 2005).
4. A. K. Gunstensen, D. H. Rothman, S. Zaleski and G. Zanetti, *Phys. Rev. A* **43**, 4320 (1991).
5. P. L. Bhatnagar, E. P. Gross and M. Krook, *Phys. Rev.* **94**, 511 (1954).
6. X. He, X. Shan and G. D. Doolen, *Phys. Rev. E* **57**, R13 (1998).
7. X. He, S. Chen and R. Zhang, *J. Comput. Phys.* **152**, 642 (1999).
8. M. R. Swift, W. R. Osborn and J. M. Yeomans, *Phys. Rev. Lett.* **75**, 830 (1995).
9. R. R. Nourgaliev, T. N. Dinh, T. G. Theofanous and D. Joseph, *Int. J. Multiphase Flow* **29**, 117 (2003).
10. X. Shan and H. Chen, *Phys. Rev. E* **49**, 2941 (1994).
11. M. Sbragaglia, R. Benzi, L. Biferali, S. Succi, K. Sugiyama and F. Toschi, *Phys. Rev. E* **75**, 026702 (2007).
12. L.-S. Luo, *Phys. Rev. Lett.* **81**, 1618 (1998).
13. T. Lee and C.-L. Lin, *Phys. Rev. E* **67**, 056703 (2003).
14. D. D'Humieres, *Rarefield Gas Dynamics: Theory and Simulations* **159**, 450 (1992).
15. P. Lallemand and L.-S. Luo, *Phys. Rev. E* **61**, 6546 (2000).
16. I. Ginzburg, *Adv. Water Res.* **28**, 1196 (2005).
17. D. D'Humieres, I. Ginzburg, M. Krafczyk, P. Lallemand and L.-S. Luo, *Philosophical Trans. Royal Soc. London* **360**, 437 (2002).
18. I. Ginzburg, *Adv. Water Res.* **28**, 1196 (2005).
19. F. J. Higuera, S. Succi and R. Benzi, *Europhys. Lett.* **9**, 345 (1989).
20. F. J. Higuera and J. Jimenez, *Europhys. Lett.* **9**, 663 (1989).
21. J. S. Wu and Y. L. Shao, *Int. J. Numer. Meth. Fluids* **46**, 921 (2004).
22. K. N. Premnath and J. Abraham, *Phys. Fluids* **17** (2005).

23. M. E. McCracken and J. Abraham, *Phys. Rev. E* **71**, 036701 (2005).
24. K. N. Premnath and J. Abraham, *Three-Dimensional Multi-Relaxation Time (MRT) Lattice-Boltzmann Models for Multiphase Flow* (Elsevier Science, 2007).
25. S. Mukherjee and J. Abraham, *Comput. Fluids* **36**, 1149 (2007).
26. I. Ginzburg, *J. Statistical Phys.* **126** (2007).
27. D. Moroni, B. Rotenberg, J.-P. Hansen, S. Succi and S. Melchionna, *Phys. Rev. E* **73** (2006).
28. P. Asinari, *Phys. Rev. E* **73**, 1539 (2006).
29. R. Benzi, S. Succi and M. Vergassola, *Phys. Rep.* **222** (1992).
30. L. Landau and E. Lifshitz, *Fluid Mechanics* (Pergamon, Oxford, 1987).